Control Engineering Practice 77 (2018) 1–14

Contents lists available at ScienceDirect

Control Engineering Practice

journal homepage: www.elsevier.com/locate/conengprac

Reliable state of charge and state of health estimation using the smooth variable structure filter

Hamed Hossein Afshari [a,*], Mina Attari [a], Ryan Ahmed [a], Ali Delbari [a], Saeid Habibi [a], Tina Shoa [b]

[a] Centre for Mechatronics and Hybrid Technology, McMaster University, Hamilton, ON, Canada
[b] Cadex Electronics Inc., Vancouver, BC, Canada

ARTICLE INFO

Keywords:
State of charge estimation
Smooth variable structure filter
Modeling uncertainty
Experimental study

ABSTRACT

This paper introduces a reliable strategy for the state of charge (SOC) and the state of health (SOH) estimation of healthy and aged Lithium polymer cells. Dynamics of the cell are modeled using some equivalent circuit models and parameters of each model are calculated by adaptive particle swarm optimization. The modeling process involves modeling and parametric uncertainties as well as measurement and instrumentation noise. They may degrade the performance of an optimal filter for SOC and SOH estimation. To alleviate effects of such uncertain factors, the smooth variable structure filter (SVSF) is implemented. The SVSF is a novel robust state estimation method that benefits from the robustness property of variable structure systems. The performance of the SVSF is compared with the extended Kalman filter (EKF) for real-time SOC estimation of a healthy and an aged Lithium polymer cell. The paper moreover presents a novel method for SOH estimation using the SVSF's chattering signal and without the need for modeling the cell undergoes aging. Experiments show performance benefits of the SVSF for reliable SOC and SOH estimation of healthy and aged Lithium polymer cells.

1. Introduction

Li-Ion batteries are increasingly used in energy storage devices for applications such as electric vehicles, cell phones, laptops, medical devices, etc. This is due to their high energy density, durability, safety, lack of hysteresis, and slow loss of charge when not in use. In order to improve the performance of Li-Ion batteries and increase their safety and efficiency, accurate management, monitoring, and control are required (Afshari, Attari, Ahmed, Farag, & Habibi, 2016). Battery management systems are designed to estimate quantities representing battery's operating conditions (e.g. state of charge (SOC), state of health (SOH), etc.) and at the same time to prevent the battery from working under dangerous situations. They accurately estimate the battery's SOC as a function of the operating time. In this context, state and parameter estimation methods are used to estimate values of the SOC and the SOH based on indirect, inaccurate and uncertain sensor measurements. Note that the accuracy of the SOC and the SOH estimation may decrease due to factors such as inaccuracies in modeling batteries, parametric variations due to aging, sensor noise, unpredictable temperature variations, hysteresis effects, unknown initial SOC, etc.

1.1. The state estimation task

State estimation is referred to as the task of calculating numeric values of hidden state variables from indirect, inaccurate and partial measurements of a system. The main objective of state estimation is to minimize the state estimation error as well as to preserve robustness versus noise, and uncertainties. The Kalman filter is the most popular method for state estimation that applies to linear systems restricted to white noise with a Gaussian distribution. The Kalman filter is a model-based estimator and provides optimal state estimates by minimizing the state error covariance matrix given a known model. For the generic case of systems with nonlinear state and/or measurement models, several numerical solutions were proposed. These solutions are generally based on linearization of the state and measurement model (e.g., the Extended Kalman filter (Afshari, Gadsden, & Habibi, 2017)) or PDF approximation (e.g., the Unscented Kalman filter (Ristic, Arulampalam, & Gordon, 2004), or the Cubature Kalman filter (Arasaratnam & Haykin, 2009)). In the extended Kalman filter (EKF), the gain is obtained by locally linearizing the state or measurement model at the operating point. The main concern with the Kalman-type filtering is the assumption of having a perfect model with known parameters. In real applications, however,

* Corresponding author.
E-mail address: h.h.afshari@gmail.com (H.H. Afshari).

https://doi.org/10.1016/j.conengprac.2018.04.015
Received 4 August 2017; Received in revised form 15 April 2018; Accepted 27 April 2018

Nomenclature

C	Capacitance element, C-rate
C_n	Nominal capacity of the cell
EKF	Extended Kalman filter
H	Linear measurement matrix
K	Filter's gain
OCV	Open circuit voltage
PSO	Particle swarm optimization
$\mathbf{Q}^{EKF}$	State error covariance for EKF
R	Resistance element
R_0	Internal resistance element
$\mathbf{R}^{EKF}$	Measurement error covariance for EKF
SOC, Z	State of charge
SOH	State of health
SVSF	Smooth variable structure filter
V	Voltage
V_t	Terminal voltage
sat()	Saturation function
sgn()	Sign function
e_x	State estimation error
e_z	Measurement error
$e_{z,k\|k}$	a priori (updated) measurement error
$e_{z,k+1\|k}$	a posteriori (predicted) measurement error
f	Nonlinear state model
i	Current
k	Discrete-time index
u	Control variable
v	Measurement noise
w	Process noise
x	State vector
$x_{k\|k}$	The *a priori* (updated) state value
$x_{k+1\|k}$	The *a posteriori* (predicted) state value
z	Measurement vector
Ξ	Chattering indicator
Δt	Sampling time
α	Scaling factor for chattering indicator
γ	Convergence rate
η	Coulombic efficiency of the cell
β	Existence boundary layer
ψ	Smoothing boundary layer
$\hat{\square}$	Estimated quantity
$\square^+$	Pseudo-inverse operator

there may be considerable uncertainties about the model structure, physical parameters, noise, and initial conditions. These factors may significantly degrade the Kalman filter's performance from its optimal solution.

To overcome or at least decrease effects of such factors on the estimator's performance, robust state estimation is proposed in which the filter is insensitive to a wider range of noise and uncertainties. There is a large number of publications in the literature devoted to design of robust state estimators for systems with norm-bounded noise and uncertainties, such as minimax estimators (Krener, 1980), considering the worst case scenario for state estimation, e.g. the H_∞ filter (Zames, 1981), or set-membership estimators (Milanese & Tempo, 1985). There are some robust estimation methods mainly based on applying a technique to robustify the Kalman filter (Gandhi & Mili, 2010). Robust Kalman filters (Gandhi & Mili, 2010) are applied to systems with norm-bounded modeling uncertainties in which an upper bound of the mean square estimation error is minimized. Robust state estimation may be achieved by means of the variable structure filtering (Gadsden & Habibi, 2013; Habibi, 2007). The smooth variable structure filter (SVSF) (Habibi, 2007) is a relatively new robust state estimation that benefits from the robustness property of variable structure systems. It guarantees the stability of state estimates by applying a discontinuous gain and pushing the measurement error to zero (Habibi, 2007). Afshari, Al-Ani, and Habibi (2015) and Afshari, Gadsden, and Habibi (2018) have introduced a second-order state estimation method that works similar to the SVSF method, but instead of using a smoothing boundary layer for chattering removal, it applies a second-order time-difference condition. They also overviewed main Gaussian filters applied for state and parameter estimation (Afshari et al., 2017).

1.2. Modeling Lithium-Ion batteries

In order to apply a model-based filter (e.g. Kalman filter, SVSF, etc.) for the SOC and SOH estimation, dynamics of the battery need to be modeled. Several methods have been reported in the literature for modeling Li-Ion batteries. These methods may be categorized into three main approaches that include: 1- empirical modeling, 2- equivalent circuit modeling, and 3- electrochemical modeling. Empirical models or black-box models simulate the terminal voltage behavior of Li-Ion batteries without the need for considering the underlying physics or any electrochemical reactions that may happen within the cells. These models are mainly based on a series of math functions with unknown parameters. Values of these parameters can be calculated using a set of input–output data and an optimization method. The optimization method calculates the unknown parameters by minimizing the output error that is the difference between the simulated and the measured output (terminal voltage).

Equivalent circuit models use lumped-element components such as resistors and capacitors to simulate dynamics of a cell. Based on the different levels of modeling complexity, they may include first-order, second-order, or third-order resistor–capacitor elements in addition to an element that represents the hysteresis effect. They do not model the cell's underlying chemistry. In contrast, the electrochemical modeling approach considers the electrochemical reactions happening inside a cell. They simulate the internal electrochemical dynamics of the cell using a set of partial differential equations. Electrochemical modeling is the most accurate approach, while it is computationally more expensive. Several techniques have been reported in the literature in order to simplify electrochemical models and apply them to real-time implementations. Note that however, the choice among these three modeling approaches is a compromise between modeling complexity, accuracy, and computational cost (Afshari, Attari et al., 2016).

The equivalent circuit approach is one of the most popular approaches for modeling Li-Ion batteries. It is because a circuit model may be rather simple, e.g. only has a voltage source and a variable resistance, or maybe complex given local conditions in a spatially-resolved model (Plett, 2004b). This approach uses a group of resistors and capacitors, where their magnitudes are obtained using an optimization method. The optimization method employs a random search at each time step to extract the parametric values such that the error between the measured terminal voltage and the simulated one is minimized. The main advantage of the equivalent circuit approach for modeling is its capability for real-time applications with an acceptable performance. The main disadvantage of this approach is its limitation for modeling the electrochemical reactions that take place internally inside the cell. This limitation prevents it from modeling some physical behaviors including the power fading, the capacity fading and more importantly the aging effect (Plett, 2004b). Ferrari-Trecate, Muselli, Liberati, and Morari (2003) have proposed a new method for the identification of hybrid systems formulated in the piecewise affine form. This method is based on the use of clustering for the classification of data points, followed by constructing a model for each cluster and linear identification of its parameters (Ferrari-Trecate et al., 2003).

1.3. Literature review

The task of real-time SOC and SOH estimation of batteries is a relatively challenging task. It is due to numerous physical and electrochemical parameters that interact together and affect the cell dynamics. There are a large number of sophisticated phenomena that may affect the cell behavior under certain conditions. They include self-discharging, aging effects, the imbalance between cells, capacity fade, and temperature-dependent factors (Samadani, Fraser, & Fowler, 2012). Hu, Li, and Peng (2012) presented a comparative study of different approaches for modeling Li-Ion cells. They used six empirical models as well as six equivalent circuit models to simulate cell dynamics with different levels of complexity (Hu et al., 2012). Plett presented a detailed procedure for modeling, parametrization, and SOC estimation of Li-Ion batteries in three publications (Plett, 2004a, 2004b, 2004c). Plett introduced a general background on battery management systems and further requirements for SOC estimation in part 1 (Plett, 2004a). He reviewed some of the main techniques presented in the literature for modeling and parameter identification of Li-Ion Polymer cells in part 2 (Plett, 2004b). Plett also applied the extended Kalman filter (EKF) for SOC estimation of a cell in part 3 (Plett, 2004c). Gomez, Nelson, Kalu, Weatherspoon, and Zhang (2011) have presented a temperature dependent equivalent circuit model that accounts for both temperature and SOC.

Chen et al. (2016) have introduced a robust sliding mode observer for SOC estimation of lithium polymer cells that were modeled using the equivalent circuit approach. They moreover employed a Neural Network technique to tune an upper bound for uncertainties within the battery model. This technique applies a switching gain based on values of the upper bound in order to cancel the SOC estimation error (Chen et al., 2016). More recently, Zhao, Duncan, and Howey (2017) investigated the observability of equivalent circuit models for Li-Ion batteries and introduced a method to estimate their SOC in the presence of sensor biases. Lashway and Mohammed (2016) implemented an adaptive strategy for the health monitoring and performance analysis of Lead-Acid and Li-Ion cells. They developed an adaptive Coulomb counting method that accounted for the shift in the SOH estimates during cycling tests (Lashway & Mohammed, 2016).

Rahimi-Eichi, Baronti, and Chow (2014) have presented an online adaptive parameter identification technique for the SOC of lithium polymer cells. They used the piecewise linear approximation to interpolate the nonlinear relationship between the open circuit voltage and the SOC in the equivalent circuit modeling context. Their technique employed the moving window least squares method for adapting parameters of the battery model (Rahimi-Eichi et al., 2014). Kim and Cho (2011) have introduced a novel SOC and SOH estimation method by combining the EKF with a per-unit system. This method used the statistical analysis of the voltage patterns in order to update the model's parameters affected by aging (Kim & Cho, 2011). Afshari, Ahmed, Farag, and Habibi (2016) and Ahmed, El-Sayed, Arasaratnam, and Habibi (2014) have presented a new strategy for electrochemical modeling of Lithium Iron Phosphate cells using the averaged single particle model (Afshari, Ahmed et al., 2016; Ahmed, El-Sayed, Arasaratnam, Habibi et al., 2014). They applied the final value theorem within the state estimation method in order to estimate the initial SOC at different layers of the cell (Ahmed, El-Sayed, Arasaratnam, Tjong, & Habibi, 2014). Afshari et al. have researched on model-based methods for health monitoring of industrial systems (Afshari, Al-Ani, & Habibi, 2014; Afshari et al., 2015; Afshari, Gadsden, & Habibi, 2014).

1.4. Contributions

This paper presents a detailed procedure for modeling, parametrization, as well as SOC and SOH estimation of a Lithium polymer cell using an equivalent circuit model. A battery test setup is designed and built to conduct a set of experiments required for modeling and parametrization. The first contribution of this paper is to implement the robust SVSF method for real-time SOC estimation of healthy and aged Lithium polymer cells. The accuracy and robustness of the SVSF are then compared with the EKF for a healthy cell with a known model and an aged cell with an uncertain model. The second contribution is to introduce and implement a novel SOH estimation technique using equivalent circuit modeling. The SOH is precisely estimated by analyzing the SVSF's secondary indicator referred to as chattering. This indicator can be used to measure uncertainties for systems under fault or any abnormal conditions. This indicator is used to estimate the SOH of a cell undergoes aging without the need for modeling the aged cell. Fig. 1 presents main steps of the process for SOC and SOH estimation using the SVSF method.

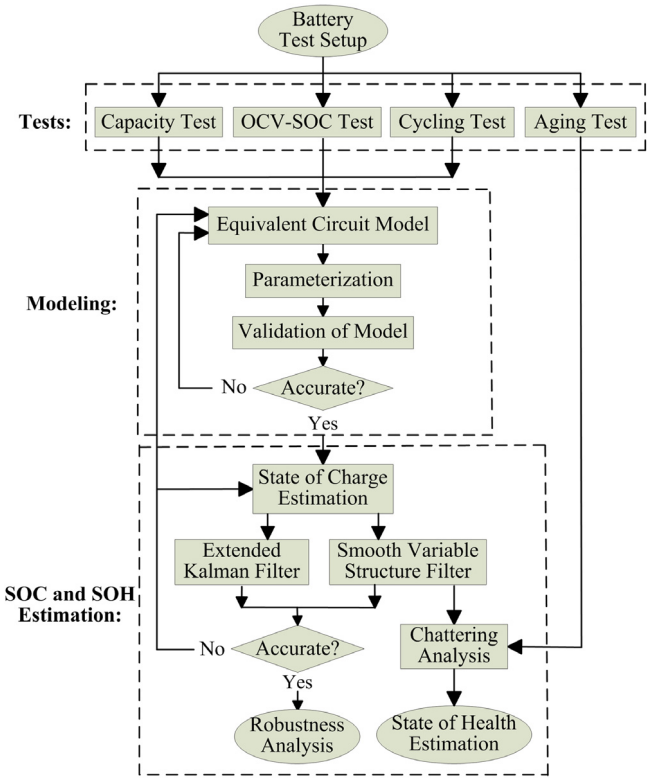

Fig. 1. Main steps of the process for SOC and SOH estimation using SVSF.

2. The Smooth Variable Structure Filter (SVSF) vs. Extended Kalman Filter (EKF)

The Kalman-type state estimation approach is referred to as a class of optimal (or near-optimal) recursive Bayesian filters restricted to systems with Gaussian noise distributions. The Kalman filter itself is an optimal state estimation method that applies to systems with a linear state and a linear measurement model restricted to Gaussian noise distributions. Based on the *a prior* knowledge of the system's model and the uncertain measurements, the Kalman filter recursively estimates the states by minimizing the covariance of the state estimation error (Afshari et al., 2017). The extended Kalman filter (EKF) is an extension to the Kalman filter that applies to systems with nonlinear state and/or measurement models and provides near-optimal state estimates. The EKF is formulated based on the local linearization of the nonlinear state and/or measurement models using the Taylor series expansion. The linearization results in the recursive calculation of the Jacobians for the nonlinear state and/or measurement models, whereas the state estimates are not optimal in the mean square error sense (Afshari et al., 2017).

The SVSF is a model-based robust state estimation method that can be used to estimate state variables of smooth nonlinear dynamic systems. It has an inherent switching action that ensures convergence of the state estimates to within a region of the real values. The switching characteristic of the SVSF is due to a discontinuous gain which provides robustness to bounded uncertainties (Habibi, 2007). Consider a discrete system with a nonlinear state model and a linear measurement model, as follows:

$$\mathbf{x}_{k+1} = \mathbf{f}(\mathbf{x}_k, \mathbf{u}_k, \mathbf{w}_k), \tag{1}$$

$$\mathbf{z}_{k+1} = \mathbf{H}\mathbf{x}_{k+1} + \mathbf{v}_k, \tag{2}$$

where $mathbf x_k$, $\mathbf{u}_k$, and $\mathbf{z}_k$ are the state, input, and measurement vectors at time step k, respectively. $\mathbf{w}_k$ and $\mathbf{v}_k$ are the bounded process and the measurement noise, respectively. In addition, $\mathbf{f}$ is the nonlinear state function and $\mathbf{H}$ is the measurement matrix. The SVSF is recursive and is summarized as follows:

1. Prediction Step (Habibi, 2007):
   • Calculation of *a priori* state and measurement estimates:

$$\hat{\mathbf{x}}_{k+1|k} = \hat{\mathbf{f}}(\mathbf{x}_k, \mathbf{u}_k), \tag{3}$$

$$\hat{\mathbf{z}}_{k+1|k} = \hat{\mathbf{H}}\mathbf{x}_{k+1|k}, \tag{4}$$

where $\hat{\mathbf{x}}$ and $\hat{\mathbf{z}}$ are the estimated state and measurement vector, $\hat{\mathbf{f}}$ and $\hat{\mathbf{H}}$are the estimated state and measurement models. The *a priori* and *a posteriori* measurement error are given by:

$$\mathbf{e}_{\mathbf{z}_{k|k}} = \mathbf{z}_k - \hat{\mathbf{H}}\hat{\mathbf{x}}_{k|k}, \tag{5}$$

$$\mathbf{e}_{\mathbf{z}_{k+1|k}} = \mathbf{z}_{k+1} - \hat{\mathbf{H}}\hat{\mathbf{x}}_{k+1|k}. \tag{6}$$

2. Update Step (Habibi, 2007):
   • Calculation of the SVSF's corrective gain, as follows (Habibi, 2007):

$$\mathbf{K}_{k+1} = \hat{\mathbf{H}}^{+}\left(\left|\mathbf{e}_{\mathbf{z},k+1|k}\right| + \gamma\left|\mathbf{e}_{\mathbf{z},k|k}\right|\right) \circ \mathrm{sgn}(\mathbf{e}_{\mathbf{z},k+1|k}), \tag{7}$$

where sgn denotes the signum function, π_{ij} is the Schur product (element-wise multiplication), and $\sum_{j=1}^{r}\pi_{ij}(k) = 1$ is the pseudo-inverse transform. Moreover, γ is a positive coefficient and denotes the convergence rate of the SVSF method (Habibi, 2007).

   • Update the *a priori* state estimate to the *a posteriori* estimate (Habibi, 2007):

$$\hat{\mathbf{x}}_{k+1|k+1} = \hat{\mathbf{x}}_{k+1|k} + \mathbf{K}_{k+1}. \tag{8}$$

The discontinuous corrective action of the SVSF gain generates high-frequency chattering that degrades the estimation performance. To suppress the undesirable chattering effects from state estimates, a smoothing boundary layer is introduced into the filter formulation such that (Habibi, 2007):

$$\mathbf{K}_{k+1} = \hat{\mathbf{H}}^{+}(|\mathbf{e}_{\mathbf{z},k+1|k}| + \gamma|\mathbf{e}_{\mathbf{z},k|k}|) \circ sat(\mathbf{e}_{\mathbf{z},k+1|k}, \boldsymbol{\psi}), \tag{9}$$

where $\boldsymbol{\psi}$ is a diagonal matrix with constant entries and denotes the smoothing boundary layer widths. In the new formulation, the sign function is replaced with a saturation function that interpolates the discontinuous action of the gain in a vicinity of the sliding hyperplane. Hence, outside the smoothing layer ψ_i (corresponding to the ith entry) the signum function applies to preserve stability. Otherwise, inside the smoothing layer ψ_i, the saturation function applies to interpolate the signum function and suppress chattering. The saturation function is given by (Habibi, 2007):

$$sat(e_{z_i,k+1|k}, \psi_i) = \begin{cases} 1 & e_{z_i,k+1|k} \geq \psi_i \\ e_{z_i,k+1|k} & -\psi_i \leq e_{z_i,k+1|k} \leq \psi_i \\ -1 & e_{z_i,k+1|k} \leq -\psi_i \end{cases}. \tag{10}$$

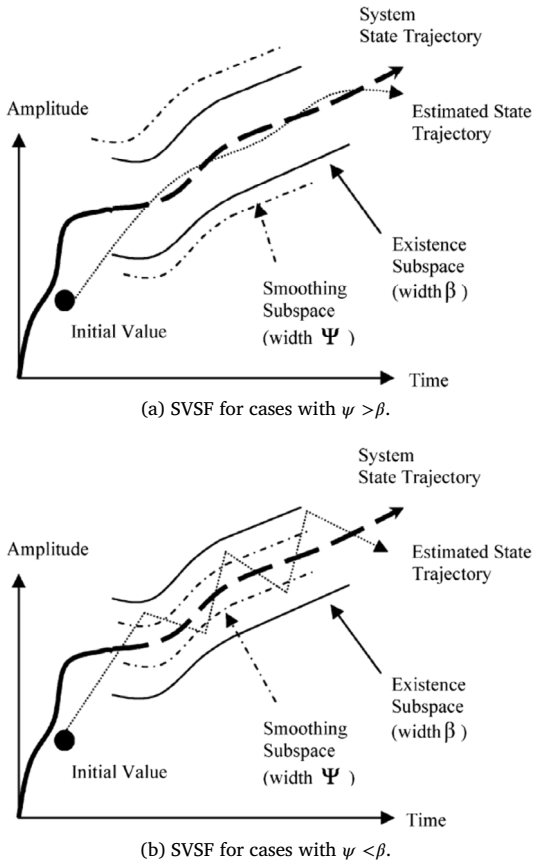

Fig. 2. The main concept of the existing and the smoothing layers in SVSF (Habibi, 2007).

Fig. 2 shows the main concept of the SVSF method for state estimation. The system state trajectory, estimated state trajectory, and existence subspace versus time are also presented in this representation. In order to start the estimation process, an initial value is selected for the state estimation process based on a prior knowledge of the systems. Thereafter, the estimated state is pushed towards a neighborhood of the system's true value referred to as the existence subspace. Once the value enters into the existence subspace, the estimated state is forced into switching along the system state trajectory via the SVSF's gain. The estimated state trajectory remains within the existing subspace that has a width proportional to modeling and parametric uncertainties, measurement noise, and disturbances. The corrective gain of the SVSF is designed based on a positive definite Lyapunov candidate given by: $V = {e_{i,z_{k|k}}}^2$. It is shown that the SVSF is stable and convergent if $|e_{i,z_{k+1|k+1}}| < |e_{i,z_{k|k}}|$ (Habibi, 2007).

There are two different boundary layers in the SVSF method including the existence layer, and the smoothing layer. The existence layer is defined in the close vicinity of the estimated state trajectory in which the stability of the estimation process is guaranteed. The width of the existence layer varies in time as a function of modeling uncertainties. Although the width of the existence layer is unknown, it is possible to obtain an upper boundary $\boldsymbol{\beta}$ for it. Moreover, the smoothing layer is defined to approximate the sign function in the corrective gain formulation and filter out chattering. Its width is known as $\boldsymbol{\psi}$ and outside this layer, the sign function is applied to achieve the stability, while inside the smoothing layer the discontinuity of the gain is interpolated by the saturation function to provide smooth state estimates. As presented in Fig. 2(a), when the smoothing layer width is larger than the existence layer width $\psi_i > \beta_i$, chattering is filtered out. Otherwise as presented in Fig. 2(b), if the smoothing layer width is

smaller than the existence layer width $\psi_i < \beta_i$, then the smoothing layer will be ineffective and chattering will appear (Habibi, 2007).

Main performance benefits of the SVSF over conventional estimation methods are:

(a) The Kalman-type filtering is formulated based on the exact knowledge of the system's model. Under real practical applications, there may be considerable noise and uncertainties, particularly when the system is going under aging, fault conditions, or any abnormal behaviors. In such cases, the system's model is not accurate and this may significantly degrade the performance of Kalman-type filtering. Otherwise, the SVSF preserves robustness and stability within a predefined boundary layer for bounded uncertainties and noise levels. Therefore, the SVSF alleviates the need for an accurate model under uncertain cases.

(b) Conventional state estimation approaches (e.g. the Kalman-type filtering, the H_∞ filter, and the particle filter) provide the measurement error (the innovation sequence) as an indicator of performance. Further to this, the SVSF provides a secondary indicator of performance based on the chattering signal (Habibi, 2007), which explicitly relates to uncertainties and modeling errors. This indicator may be interpreted to monitor the system's health condition.

(c) The EKF applies to estimate states of nonlinear systems based on the local linearization of nonlinearities around operating points. This, however, reduces the accuracy as well as the optimality of the filter, particularly under uncertain cases. Otherwise, the SVSF estimates the states using the nonlinear state model and without the need for linearization or approximation. This alternatively increases the accuracy of the estimation. Note that however for systems with nonlinear measurement models, similar to the Kalman-type filtering, the SVSF needs to locally linearize the nonlinearities around operating points.

3. The battery test setup and performance tests

In order to conduct experiments on a Lithium polymer cell, a battery test setup is designed and built. Data collected from these tests are used for modeling and parametrization of the cell, and later on, for the SOC and SOH estimation.

3.1. The battery test setup

The battery test setup is as shown in Fig. 3. The battery test setup includes a Lithium polymer cell, an environmental chamber, a power supply, a data acquisition system, a current sensor, thermocouples and a safety circuit. The power supply is able to provide ±6 V and ±150 A. It is connected directly to the Li-Ion cell for charging and discharging and controlled using the computer via connections to the data acquisition chassis. Voltage, current, and temperature measurements are acquired at a sampling frequency of 16 Hz. The 8-slot Ethernet chassis used is the NI cDAQ-9188. Analog Input modules, Analog Output modules, and thermocouple modules are incorporated within the chassis. A safety circuit was used in order to cut off power from power supply to the battery if MAX/MIN allowable voltage, current and temperature limits are exceeded. Allowable limits are set using potentiometers.

The environmental chamber is able to vary temperature between — 66 °C to 177 °C. The environmental chamber uses two 2.5 HP compressors in order to change temperature within its chamber. Current is measured using a highly accurate hall-effect current sensor (LEM IT 200-S Ultra Slab). Fig. 4 shows four omega type-T thermocouples that are used to monitor and record temperature. Three thermocouples are used for monitoring battery temperature and one was used for ambient temperature measurements. A rechargeable Lithium polymer cell is used for test, modeling, and estimation. Table 1 presents cell properties as provided by the manufacturer.

Fig. 3. Main components of the battery test setup located at CMHT.

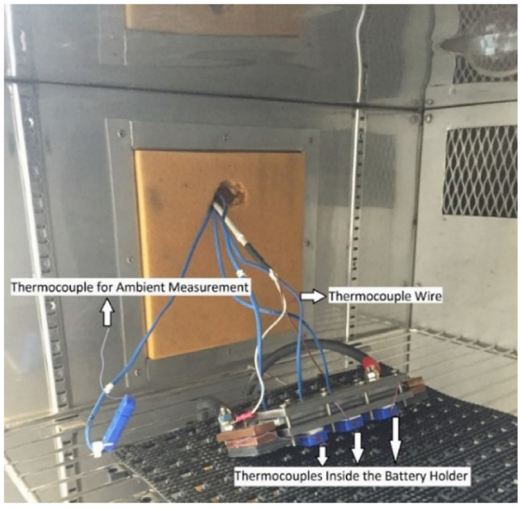

Fig. 4. Thermocouple connections inside the chamber.

Table 1
Physical characteristics of the Lithium Polymer Cell.

Parameter condition		Numeric value
Capacity	Minimum	2.00 Ah
Cell voltage	Nominal	3.6 V
	Charge	4.2 V
	Discharge	2.0 V
Charge current	Standard	2.0 A
	Maximum	6.0 A
Charge time	Standard	1.5 h
Discharge current	Standard	2.0 A
	Maximum	20.0 A

3.2. Test procedures

Some tests are conducted to specify cell's baseline characteristics such as capacity, internal resistance, open-circuit voltage versus the SOC, as well as aging effects. The first three tests are referred to as the reference performance tests and are performed on a fresh cell at a controlled room temperature of 25 °C. The fourth test is the aging test and is conducted to study the effect of battery degradation due to multiple charging/discharging. The guideline for these tests is prepared based on a report published by the U.S. Idaho National Laboratory (The U.S. DOE/Idaho National Laboratory, 2008).

These tests are described and conducted as follows:

1—The Static Capacity Test:

The static capacity test is conducted to measure the cell capacity in Ampere-hours at a constant current discharge rate. It provides a baseline for measuring the nominal capacity of a fresh cell. This test applies based on the constant-current constant-voltage mode, as follows (The U.S. DOE/Idaho National Laboratory, 2008):

(a) Charge the Li-Ion cell at 1 C-rate (2 A) in a constant-current constant-voltage mode to reach the fully charged state. The cell will be fully charged at 4.2 V and the test will stop when the current is at 0.02 C (0.04 A);
(b) Disconnect the cell and leave it to rest with no load for one hour in order to stabilize the voltage and the current;
(c) Discharge the cell at 1 C-rate with a constant current until the cell voltage hits the cell minimum voltage limit at 2 V;
(d) Disconnect the cell and leave it to rest with no load for one hour.

The static capacity test was conducted based on the above procedure, and the current was recorded. Taking the numerical integration of the current over time, the nominal capacity C_n of the cell was obtained equal to 2.05 Ah (7380 A s) and it is close to the manufacturer data (see Table 1).

2—The OCV–SOC Characterization Test:

The OCV–SOC characterization test is conducted to characterize the open-circuit voltage (OCV) as a function of the state of charge (SOC) variations. In order to minimize the cell dynamics, as well as the Ohmic loss produced by the battery internal resistance, a very small C-rate (C/20, C/15) is applied for the OCV–SOC characterization test. In this context, by performing this experiment with very small C-rates, the measured terminal voltage is assumed to be equal to the open circuit voltage. This test is similar to the capacity test but is conducted at a very low C-rate. The OCV–SOC characterization test is performed, as follows (The U.S. DOE/Idaho National Laboratory, 2008):

(a) Charge the cell in a CCCV mode until reaching the maximum voltage limit at 4.2 V.
(b) Discharge the cell at the constant current mode with 1 C-rate until the voltage reaches the minimum voltage limit at 2 V.
(c) Disconnect the cell from the chamber and leave it and other components of the setup to rest with no load. This causes that the cell remains at a zero state of charge.
(d) Charge the cell at a very small C-rate of C/15 (0.1333 A) in a constant-current constant-voltage mode until it hits the maximum voltage of 4.2 V. The cell is left to rest for one hour.
(e) Discharge the cell at the same rate of C/15 (0.1333 A) until and the battery hits the minimum voltage of 2 V.

The importance of the OCV–SOC characterization test is for creating the measurement model and accordingly estimating the terminal voltage. The SOC–OCV characterization test was separately conducted for charging and discharging with a low C-rate equal to C/15 (0.1333 A). Using a law C-rate for charging and discharging causes that the voltage drop due to the internal resistance of the cell will be negligible. Moreover, this minimizes battery dynamics, and hence, the measured terminal voltage can be considered as the open circuit voltage. To create the measurement model, the OCV profile needs to be formulated as a function of the SOC (or Z). The charging and discharging curves were then averaged to obtain a single fixed profile that correlated the OCV values to SOC variations. A 10th-order polynomial function was used for model parameters fitting of this profile. It is given by:

$$OCV(Z_k) = p_{10}Z_k^{10} + p_9Z_k^9 + p_8Z_k^8 + p_7Z_k^7 + p_6Z_k^6 + p_5Z_k^5 + p_4Z_k^4 + p_3Z_k^3 + p_2Z_k^2 + p_1Z_k + p_0. \quad (11)$$

Table 2 shows numeric values of the eleven coefficients obtained by interpolation. Fig. 5 shows three profiles including the OCV–SOC curve for charging, the OCV–SOC curve for discharging, and their average curve used for interpolation.

Table 2
Coefficients of the 10th-Order SOC–OCV Polynomial.

Coefficient	p_{10}	P_9	P_8	P_7
Numeric value	−10150.68	54373.42	−125525.42	163388.70
Coefficient	P_6	P_5	P_4	P_3
Numeric value	−131706.22	67987.96	−22460.65	4613.87
Coefficient	P_2	p_1	p_0	
Numeric value	−554.99	35.66	2.53	

It is deduced from Fig. 5 that the cell behavior is not identical for charging and discharging. It is because of the hysteresis effect that results in loss of energy. The amount of voltage drop by the hysteresis effect may simply be obtained by subtracting the SOC–OCV curve for discharging from the one obtained for charging. Fig. 6 shows the voltage drop due to the hysteresis effect during the OCV–SOC characterization test. This profile may be used to model the hysteresis effect.

3—The Driving Cycle Test:

In this research, two current cycles are used in order to excite the cell's dynamics. They include 1- a current cycle provided by the manufacturer, and 2- a current cycle obtained by the urban dynamometer driving schedule (UDDS) (Ahmed, El-Sayed, Arasaratnam, Habibi et al., 2014; Ahmed, El-Sayed, Arasaratnam, Tjong et al., 2014). The terminal voltage is measured as an output. Fig. 7 presents profiles of the applied input current cycle i_k, the measured terminal voltage $V_{t,k}$, and the SOC. The SOC profile is calculated though numeric integration of i_k over time (Coulomb-counting), using the following equation (Plett, 2004b):

$$Z_{k+1} = Z_k - \frac{\eta \Delta t}{C_n} i_k, \quad (12)$$

where Z_k is the state of charge, η is the Coulombic efficiency, C_n is the cell's nominal capacity, and Δt is the sampling time.

4—The Aging Test:

There is a number of procedures for conducting the aging test, as reported in The U.S. DOE/Idaho National Laboratory (2008). In this research, the aging test is designed and implemented on a fresh Lithium polymer cell following the schedule B3 test (The U.S. DOE/Idaho National Laboratory, 2008). In this test, the battery undergoes aging by applying high C-rate currents up to 10C and at elevated temperatures (35 to 40 °C). It is because chemical reactions exponentially increase with temperature, and hence, cell aging is accelerated at higher temperatures. The aging test is designed based on the manufacturer data and a mix of some current cycles (UDDS, US06, HWFET, etc.) which is used for charging/discharging. According to Table 1, since the maximum charging current is 3C, the maximum regenerative current for charging is set to 3C (6A). Moreover, the maximum discharging current is set to 10C (20A). In the conducted aging test, based on schedule B3, a charge/discharge cycle lasts for 100 min, and after each cycle, the cell is left to rest with no load for 30 min. The aging test is conducted on a fresh Lithium polymer cell for about 20 weeks. It makes the cell be aged at approximately 80% of its nominal capacity after 20 weeks. In order to measure the cell degradation, reference performance tests are conducted every 5 weeks. Fig. 8 presents the capacity degradation of the cell under the aging test-schedule B3.

4. The equivalent circuit modeling method

In this research, six equivalent circuit models are suggested for modeling and parametrization of the Lithium polymer cell with different levels of complexity. These models include the 1st-order R-RC, the 2nd-order R-2RC, and the 3rd-order R-3RC model with and without the hysteresis element. In this context, the input–output (current-terminal voltage) data are initially captured using the test setup and following the test procedures. Thereafter, the adaptive particle swarm optimization

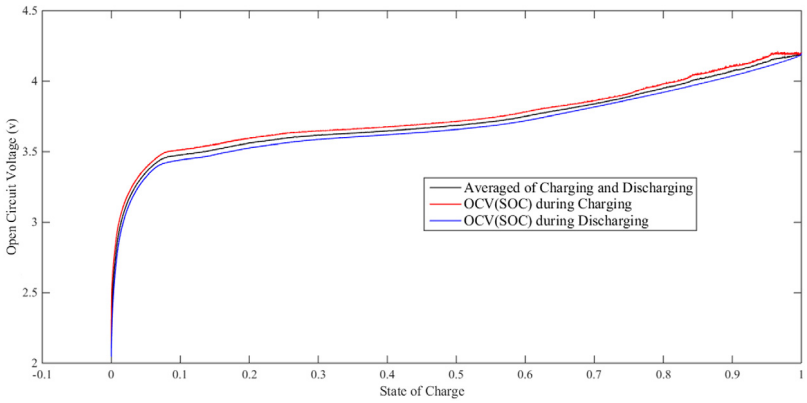

Fig. 5. Profiles of the OCV–SOC for charging, discharging, and their average.

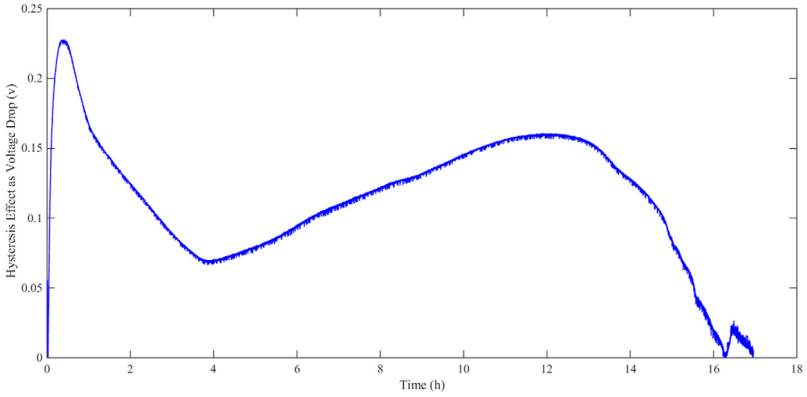

Fig. 6. Profile of the voltage drop due to hysteresis using the OCV–SOC test.

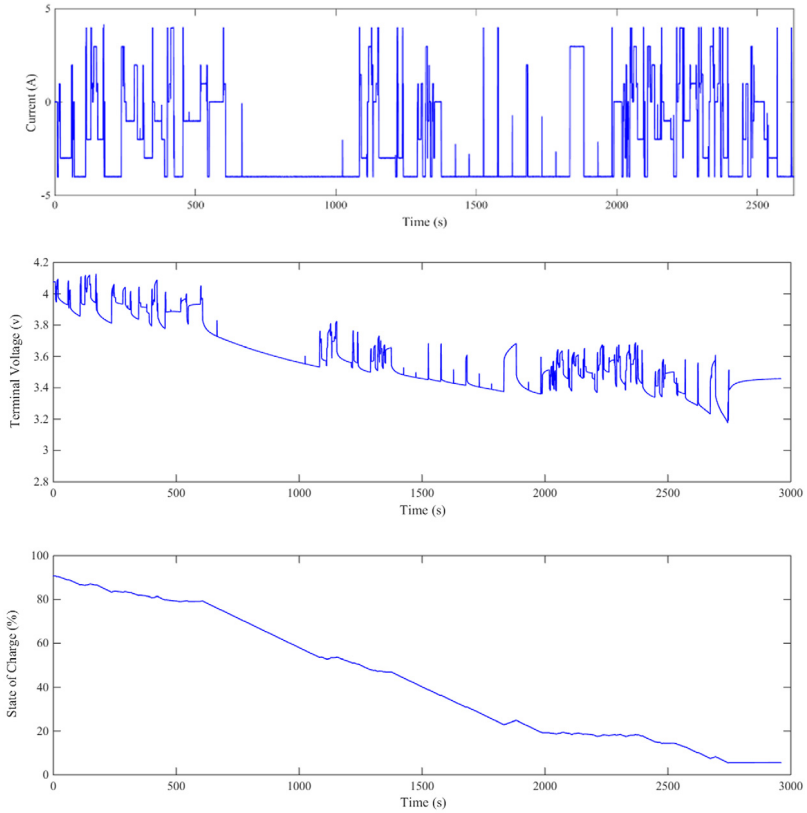

Fig. 7. Profiles of the input current cycle, measured terminal voltage, and the SOC (calculated by Coulomb counting) using the driving cycle test.

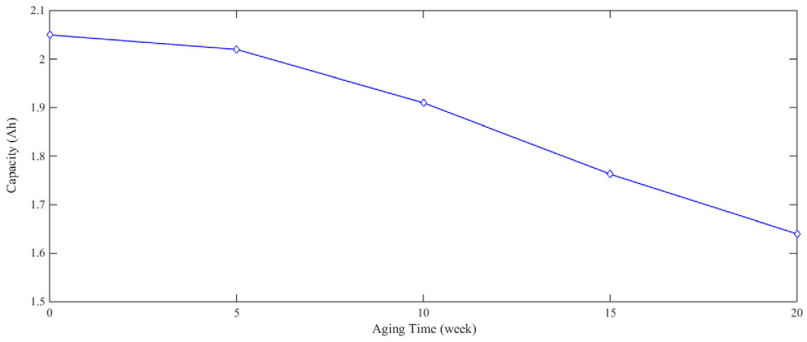

Fig. 8. The capacity degradation profile through the aging test-schedule B3.

(PSO) technique (Al-Ani, 2012) is applied to each model for parameter identification. The adaptive PSO optimizer applies a more efficient search engine with respect to a conventional optimizer such as the genetic algorithm. Due to lack of space, the paper only describes the 3rd-order R-3RC model without the hysteresis element. The performance of this model is then compared with other five equivalent circuit models in terms of accuracy and computational cost.

4.1. Adaptive particle swarm optimization

The particle swarm optimization (PSO) method is a heuristic stochastic optimization method that is originated from the swarm intelligence concept. This concept describes how a swarm of insects, a flock of birds, or a school of fish search for food. Following this concept, a PSO method uses a population-based search engine to determine an optimal set of solutions in the objective space. There is a large number of techniques that introduce modifications to the original PSO method. These modifications improve the PSO performance in terms of the convergence rate, exploration capability, and computational complexity. Al-Ani (2012) has developed the adaptive PSO concept by using an adaptive parallel clustering-based search engine into the optimizer formulation. This optimizer uses a new dynamic model for updating the velocity of particles in the search space and prevents selection of local optimums. The adaptive PSO technique can dynamically tune values of the designed parameters, search space boundaries, weighting factors, as well as the external repository's size (Al-Ani, 2012). It not only overcomes the main concerns of a heuristic optimization technique (e.g. premature convergence, diversity, quality guarantees, etc.), but also increases the optimizer convergence rate. The adaptive PSO technique (Al-Ani, 2012) is used in this research to identify parameters of the 3rd-order R-3RC model using input–output data.

4.2. The 3rd-Order R-3RC model

The 3rd-order R-3RC model consists of three elements including 1- an internal resistance R_0, 2- three modeling resistances R_1, R_2, R_3, and 3- three modeling capacitances C_1, C_2, C_3. It is formulated in the state-space form, as follows (Hu et al., 2012):

$$\begin{bmatrix} V_{1,k+1} \\ V_{2,k+1} \\ V_{3,k+1} \\ Z_{k+1} \end{bmatrix} = \begin{bmatrix} 1-\frac{\Delta t}{R_1C_1} & 0 & 0 & 0 \\ 0 & 1-\frac{\Delta t}{R_2C_2} & 0 & 0 \\ 0 & 0 & 1-\frac{\Delta t}{R_3C_3} & 0 \\ 0 & 0 & 0 & 1 \end{bmatrix} \begin{bmatrix} V_{1,k} \\ V_{2,k} \\ V_{3,k} \\ Z_k \end{bmatrix} + \begin{bmatrix} \frac{\Delta t}{C_1} \\ \frac{\Delta t}{C_2} \\ \frac{\Delta t}{C_3} \\ -\frac{\eta \Delta t}{C_n} \end{bmatrix} i_k, \tag{13}$$

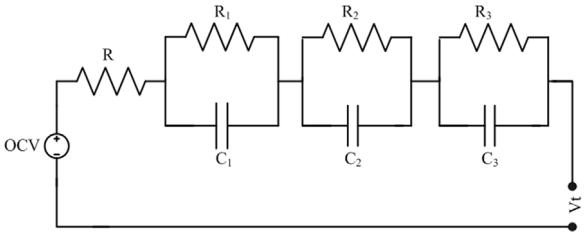

Fig. 9. The 3rd-order R-3RC model of a battery cell.

$$V_{t,k} = OCV(Z_k) - V_{1,k} - V_{2,k} - V_{3,k} - R_0 i_k, \tag{14}$$

where $V_{1,k}$, $V_{2,k}$, and $V_{3,k}$ are the voltage across capacitors C_1, C_2, and C_3, respectively. The model has four state variables: the voltage $V_{1,k}$, the voltage $V_{2,k}$, the voltage $V_{3,k}$, and the SOC variable Z_k. The input to the model is the current i_k and the output is the terminal voltage $V_{t,k}$. Moreover, the internal resistance R_0 represents the Ohmic resistance of a cell. It has two values, R_0^+ for a positive input current, and R_0^- for a negative current. $OCV(Z_k)$ represents the open-circuit voltage relationship defined as a polynomial function of Z_k. Fig. 9 shows a circuit diagram for the 3rd-order R-3RC model.

4.3. Modeling and parametrization

Modeling and parametrization of the Lithium polymer cell are performed using MATLAB. The sampling time is equal to 0.062 s, and the cell Coulombic efficiency η is assumed to be one. The nominal capacity of the cell was obtained by the static capacity test and was equal to 7380 A s. The OCV–SOC averaged curve is approximated using a 10th-order polynomial function. The adaptive PSO technique is used to identify values of the eight unknown parameters of the model including R_1, C_1, R_2, C_2, R_3, C_3, R_0^+, R_0^-. The optimizer minimizes the error that is the difference between the measured and the simulated terminal voltage. The objective function is given by:

$$J = \min \sum_{k=1}^{n} \left(V_{t,k} - \hat{V}_{t,k}\right)^2. \tag{15}$$

Table 3 lists numeric values of the eight unknown parameters calculated by the adaptive PSO technique. The adaptive PSO technique is compared to the genetic algorithm in terms of their fitness value at each generation. The fitness value may be used as an index for comparing the convergence rate of each optimizer. The population size and the generation number for both the genetic algorithm and the adaptive PSO technique are set equal to 1000 populations and 15 generations. Fig. 10 presents that for a 1000 population size and after 15 generations, the adaptive PSO technique has smaller fitness values compares to the

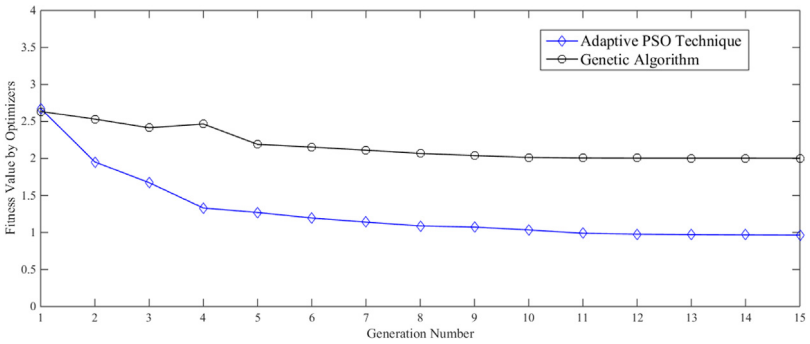

Fig. 10. Fitness values of the genetic algorithm and adaptive PSO.

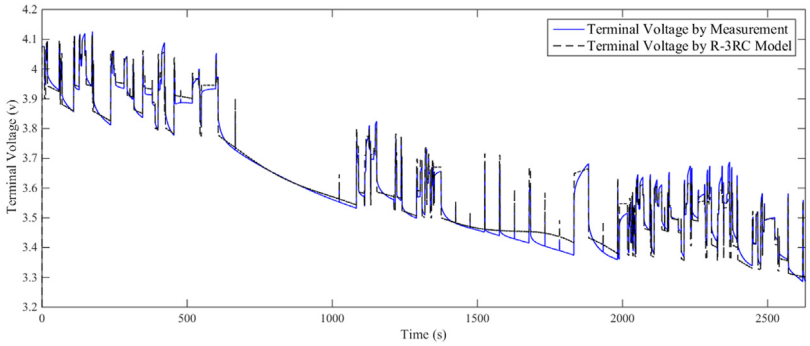

Fig. 11. Profiles of the measured and simulated terminal voltage for the model.

Table 3
Parametric values of the 3rd-order R-RC model using adaptive PSO.

Parameter	Numeric value
Modeling capacity, C_1	1293.54 (A s)
Modeling resistance, R_1	0.00634 (Ω)
Modeling capacity, C_2	12384.35 (A s)
Modeling resistance, R_2	0.00624 (Ω)
Modeling capacity, C_3	4638.46 (A s)
Modeling resistance, R_3	0.00371 (Ω)
Internal resistance, R_0^+	0.03140 (Ω)
Internal resistance, R_0^-	0.02550 (Ω)

genetic algorithm. This alternatively leads to a faster convergence rate for the adaptive PSO technique compares to the genetic algorithm.

Fig. 11 shows profiles of the measured terminal voltage and the one obtained by the 3rd-order R-3RC model. The root-mean-square (RMS) value of the error for the terminal voltage is equal to 0.01897 V. Note that the accuracy of the 3rd-order R-3RC model with the above parameters has been verified using another validation experiment. In this experiment, a UDDS cycle applies to excite the battery cell. Fig. 12 compares the measured and the simulated terminal voltage for the validation experiment. In this experiment, the RMS of the error between the measured and the simulated terminal voltage is obtained as 0.0198 V. Fig. 13 compares the accuracy of the six equivalent circuit models based on the RMS values of the output error. Fig. 13, the 3rd-order R-3RC-H model is the most accurate model, closely followed by the 3rd-order R-3RC model. Note that since the execution times for running these six models are close, the accuracy is the main parameter of interest.

5. Reliable SOC estimation using the SVSF method

Since the SOC cannot be directly measured, state estimation methods are required to extract the SOC value from terminal voltage measurements. The 3rd-order R-3RC model with parameters of Table 3 can be used by an estimator to predict SOC values. Note that there may be several sources of noise, modeling and parametric uncertainties in the SOC estimation process. The main sources of modeling uncertainties include:

- Inaccuracies in the modeling due to approximation as an equivalent circuit model;
- Averaging of the OCV–SOC curve for charging and discharging with a single curve;
- Approximating the hysteresis curve;
- Uncertainties in the initial SOC; and
- Parametrization error.

The main sources of parametric uncertainties include the error in the parameter identification of the cell and deviations of battery's parameters from their nominal values due to aging or improper usage. There are also several sources for the noise that include the instrumentation noise, the voltmeter measurement noise, and unpredictable variations of the cell temperature. To alleviate negative effects of noise, modeling and parametric uncertainties, robust state estimation techniques are proposed.

From a practical point of view, there is a trade-off between the complexity of the cell model and its accuracy. In this study, the 3rd-order R-3RC model without the hysteresis element is selected for SOC estimation. Even though the 3rd-order R-3RC-H model is slightly more accurate than the one without hysteresis; however, the 3rd-order R-3RC model without hysteresis is more suitable for real-time SOC estimation. It is because this model has a time-invariant linear state model and it is less computationally demanding. Hence, for SOC estimation, the modeling accuracy is compromised in the price of reducing the computational effort and running time. Fig. 14 shows a block-diagram scheme for the real-time SOC estimation task. It consists of the hardware and software sides. The hardware side includes the experimental battery setup, cell, measurement sensors, and a personal computer. The software side includes filtering strategies, the 3rd-order R-3RC model, and a user-interface software designed by LabVIEW.

In this research, full state estimators are designed for SOC estimation using the EKF and the SVSF method. The measurement equation of the

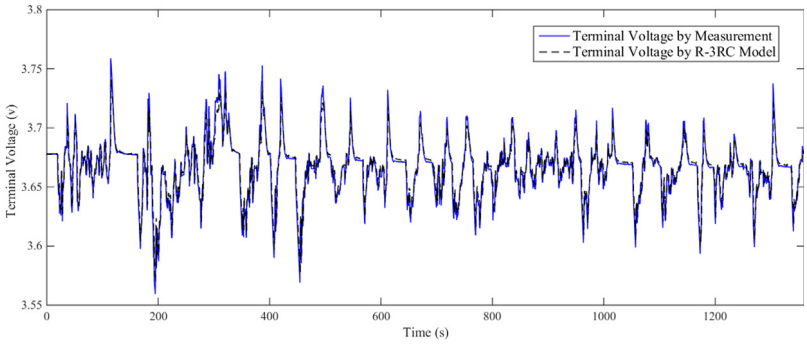

Fig. 12. Profiles of measured and simulated terminal voltage using validation test.

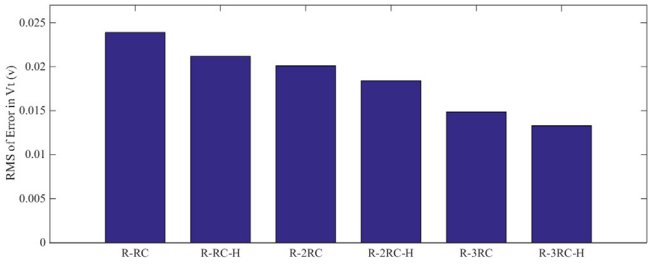

Fig. 13. Accuracy of six models in terms of RMS of the measurement error.

3rd-order R-3RC model is nonlinear and needs to be linearized with respect to the SOC variable. The Taylor's series expansion is used for linearization, whereas high-order terms are neglected. The linearized form of the measurement equation is equal to:

$$V_{t,k} = \left.\frac{\partial OCV(Z_k)}{\partial Z_k}\right|_{z_{k|k-1}} - V_{1,k} - V_{2,k} - V_{3,k} - R_0 i_k. \quad (16)$$

Since there is only one measurement V_t, the measurement error e_z and the smoothing layer width ψ are scalers. For the SVSF, the convergence rate γ is set to 0.5, and the smoothing layer width is set to 1. For the EKF, the process noise covariance $\mathbf{Q}^{\mathbf{EKF}}$ and the measurement noise covariance $\mathbf{R}^{\mathbf{EKF}}$ are respectively set to:

$$\mathbf{Q}^{EKF} = \mathbf{Diag}([1\times e-6, 1\times e-6, 1\times e-6, 1\times e-6]),\ \mathbf{R}^{EKF} = [5]. \quad (17)$$

The initial state error covariance matrix for the EKF is set to: $\mathbf{P}^{EKF}(0) = \mathbf{Diag}([0.1, 0.1, 0.1, 0.1])$. SOC values are estimated using the EKF and SVSF methods for a healthy and an aged Lithium polymer cell in three scenarios, as follows:

It is guaranteed that if the convergence rate matrix γ of the SVSF is diagonal with positive elements such that $0 \leq \gamma_{ii} < 1$, the SVSF will produce convergent state estimates (Habibi, 2007). Following the stability criterion of the SVSF (Habibi, 2007), and using the error equation of the filter, it is deduced that:

$$|e_{z_{k|k}}| = \gamma |e_{z_{k-1|k-1}}|. \quad (18)$$

Hence, the convergence rate of the SVSF is determined by the proper choice of γ such that $0 \leq \gamma_{ii} < 1$. The proper choice of γ ensures that eigenvalues of the error equation remain within the unit circle and hence guarantees the stability of state estimates.

5.1. Healthy Lithium polymer cell with known initial SOC

In this scenario, a healthy Lithium polymer cell with a perfectly known model undergoes experimentation. The actual initial SOC was equal to 90.7%, whereas for the initial SOC estimate is assumed to be 85%. Hence, the initial state estimation vector is assumed to be $\hat{\mathbf{x}}(0) = \begin{bmatrix}0 & 0 & 0 & 85\end{bmatrix}^T$ for both EKF and SVSF. Table 4 presents RMS values of the error for the SOC and the terminal voltage estimation. Fig. 15 compares the estimated SOC and the estimated terminal voltage with the actual ones using the 3rd-order R-3RC model. The actual SOC is obtained by Coulomb counting, and the actual terminal voltage is obtained by voltmeter measurements.

Table 4
RMS of error for a healthy cell with perfectly known model.

	SOC (%)	Terminal voltage (v)
EKF	0.990	0.0243
SVSF	0.999	0.0225

Table 5
RMS of error for a healthy cell with unknown initial SOC.

	SOC (%)	Terminal voltage (v)
EKF	4.858	0.0287
SVSF	3.184	0.0239

Table 6
RMS of error for the aged cell with unknown model.

	SOC (%)	Terminal voltage (v)
EKF	2.835	0.0296
SVSF	1.942	0.0237

5.2. Healthy Lithium polymer cell with unknown initial SOC

This scenario is applied to examine the robustness of state estimators versus uncertainties in the initial SOC estimate. In this scenario, the healthy Lithium polymer cell with a perfectly known model undergoes experimentation. The initial SOC estimate is assumed to be 50%, whereas the actual initial SOC is 90.7%. Table 5 compares RMS values of the error for this scenario. Fig. 16 compares profiles of the estimated SOC and the estimated terminal voltage with the actual ones.

5.3. Aged Lithium polymer cell with unknown model

This scenario is applied to examine the robustness of estimators versus unknown uncertainties. In this scenario, an aged Lithium polymer cell with an unknown model undergoes experiments. The capacitance of the aged cell is equal to 6260 A s (SOH = 80%). To compare the robustness of the SVSF with the EKF, the 3rd-order R-3RC model with parameters of Table 3 is used for SOC estimation, whereas terminal voltage data are obtained from the aged cell. Table 6 compares RMS values of the error for this scenario. Fig. 17 compares profiles of estimated SOC and terminal voltage with the actual ones.

According to Figs. 15, 16 and 17, it is deduced that where the cell model, parametric values, and the initial condition are accurate (scenario *A*), the SVSF accuracy is close to the EKF for SOC estimation.

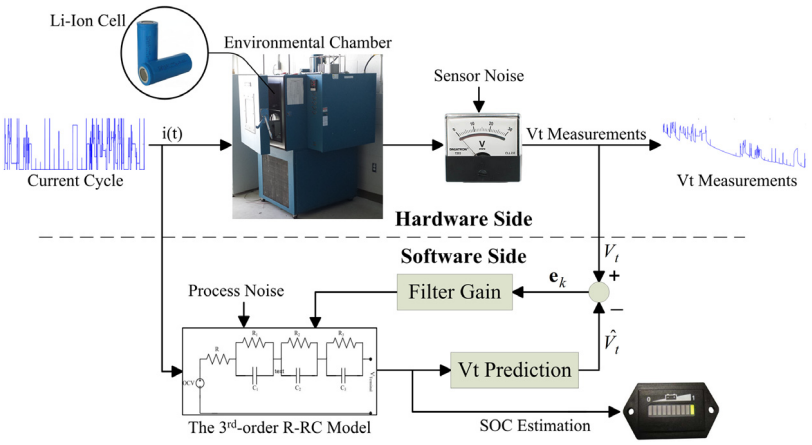

Fig. 14. A general scheme of the reliable strategy for SOC estimation.

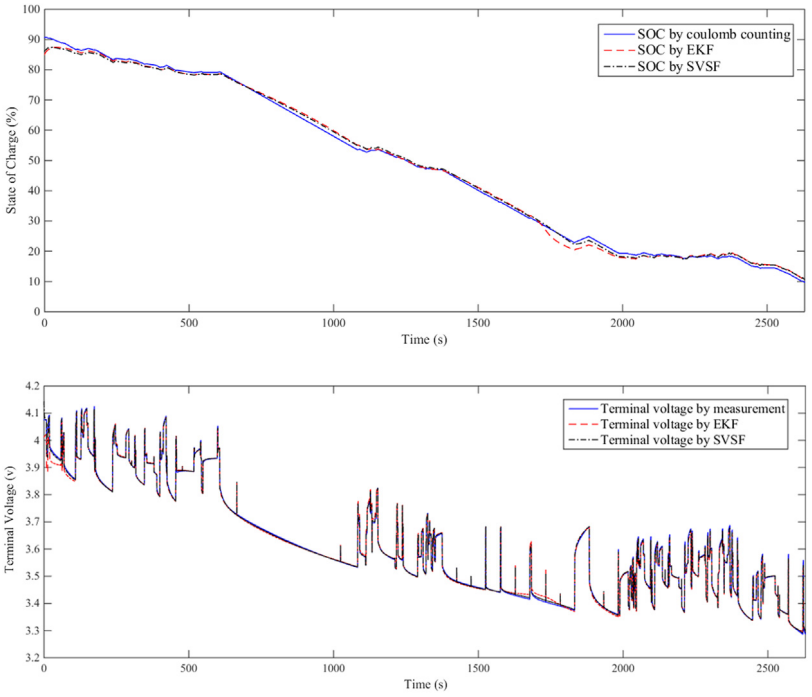

Fig. 15. The actual and the estimated SOC and terminal voltage profiles for a healthy Lithium polymer cell with initial SOC estimate equal to 85%.

Otherwise, where there exist uncertainties in the initial condition (scenario *B*) or in modeling and parametric values (scenario *C*), the SVSF method provides more accurate SOC estimation. Moreover, for these scenarios, the SVSF is more accurate for terminal voltage estimation. The computational cost for the SVSF is less than the EKF, and both methods can be applied for real-time SOC estimation.

6. SOH estimation based on the chattering analysis

Further to the measurement error (the innovation sequence), the SVSF method provides a second performance indicator that is referred to as the chattering indicator. Chattering reflects the level of modeling and/or parametric uncertainties within the system model. Statistical properties of the chattering signal significantly change for systems under a fault or any abnormal conditions. In such cases, since state estimators use the normal model of the system, modeling and/or parametric uncertainties increase considerably. Hence, the chattering indicator may be used as a tool for health monitoring, and even for quantifying the severity of the fault condition. Note that for SOC estimation using the SVSF, chattering was initially alleviated by means of the smoothing layer concept. To introduce chattering as a performance indicator, the width of the smoothing layer needs to be set equal to a small value. It is because a smoothing layer with a large width will filter out useful information from the chattering signal. The chattering indicator is given by (Habibi, 2007):

$$\Xi = \begin{cases} 0 & \text{for } |e_{i,z_{k|k}}| \le \psi_i \\ \alpha\left(e_{i,z_{k|k}} - \psi_i\right)^2 & \text{for } |e_{i,z_{k|k}}| > \psi_i \end{cases}, \tag{19}$$

where ψ_i denotes an entry of the diagonal smoothing layer width matrix Ψ, $e_{i,z_{k|k}}$ is an entry of the measurement error vector, and α is a scaling coefficient. Since there is only one measurement, the measurement error e_z and the smoothing layer width ψ are scalers. In order to use the SVSF's chattering indicator for SOH estimation, ψ and α are set to 10^{-3} and 10^4, respectively.

Five cases are studied for SOH estimation including the healthy Lithium polymer cell, and the aged one with four levels of aging. The

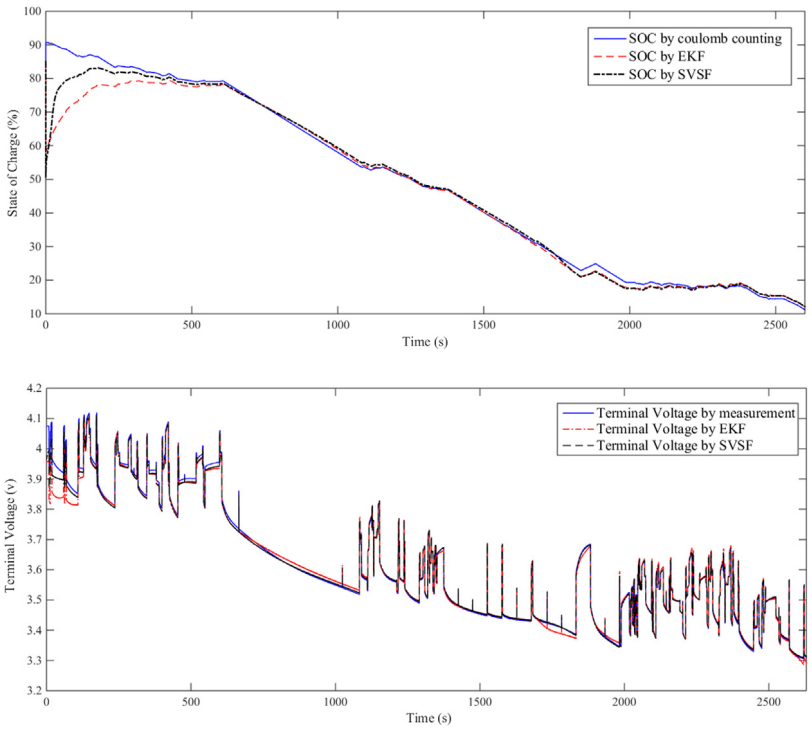

Fig. 16. The actual and the estimated SOC and terminal voltage profiles for a healthy Lithium polymer cell with initial SOC estimate equal to 50%.

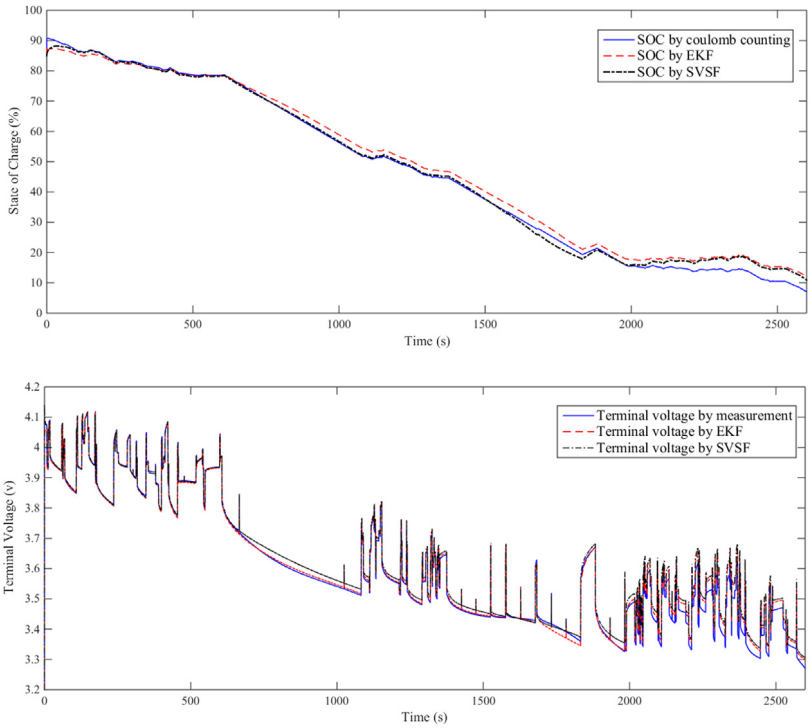

Fig. 17. The actual and the estimated SOC and terminal voltage profiles for the aged Lithium polymer cell with an unknown model.

four aging levels include aging after 5 weeks, 10 weeks, 15 weeks, and 20 weeks (see Fig. 8). The normal 3rd-order R-3RC model is used by the SVSF to generate chattering, whereas the terminal voltage is measured for each case separately. The chattering signal is captured for each case and is analyzed to estimate the SOH of the Lithium polymer cell under aging. The static capacity test is conducted after every five weeks to measure the capacitance degradation during aging. Fig. 18 shows profiles of the chattering indicator for the healthy Lithium polymer and the one under aging after 20 weeks. Fig. 18 presents that the indicator's amplitude for the cell under aging is much larger than the healthy cell (about 60 times). Table 7 presents mean and standard deviations (STD) values of the chattering indicator relevant to each case. It also presents the cell capacitance for each case obtained by the static capacity test.

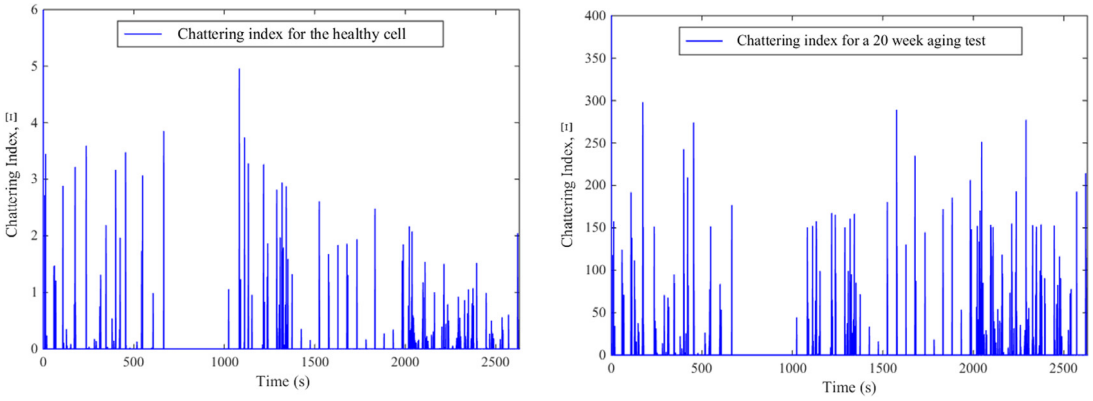

Fig. 18. Chattering indicators for a healthy and an aged (20 weeks aging) cell.

Table 7
The SVSF's chattering as an indicator for SOH estimation.

Cell test case	Cell capacitance (A s)	Statistical properties of Ξ	
		Mean	STD
Healthy cell	7380	0.0043	0.0877
After 5 weeks aging test	7272	0.1644	1.7687
After 10 weeks aging test	6876	0.4145	4.8632
After 15 weeks aging test	6347	0.6306	7.3245
After 20 weeks aging test	5905	0.8283	9.5857

The mean and standard deviation values may be used to quantify the capacity degradation due to aging.

Table 7, it is deduced that the mean and the standard deviation value of the chattering indicator increases when the cell undergoes aging. A longer aging test results in higher mean and standard deviations values for the chattering indicator. Alternatively, it may be used to estimate the current SOH of the cell without the need to obtain a new model and parameterize it for the aged cell. Introducing the SVSF's chattering indicator for SOH estimation based on an equivalent circuit model obtained for the healthy cell is another main advantage of the SVSF for SOC estimation. It also alleviates the need to study the electrochemical reactions inside a cell in order to calculate its SOH.

7. Conclusion

This paper introduces a new reliable strategy for the real-time state of charge (SOC) and state of health (SOH) estimation of Lithium polymer cells. The paper describes a battery test setup and a general guideline for conducting reference performance tests. Results of these tests are later used to obtain six equivalent circuit models that describe the cell dynamics with different levels of complexity. These models are then parameterized using experimental input–output data and the adaptive particle swarm optimization method. Precise modeling of a battery requires extensive and complicated equations which might not be practically tractable. The equivalent circuit models impose a modeling uncertainty to the estimation process in the first place, apart from other sources of uncertainty and noise.

The SVSF and the EKF methods are applied to these models in order to estimate the SOC and the terminal voltage of the healthy and aged cells. Due to the unique design of the SVSF method for state estimation, it becomes inherently robust and stable to uncertainties. This characteristic is specifically invaluable for SOC estimation of batteries. Two sources of uncertainties are investigated for SOC estimation that included uncertainties on the initial SOC estimate and on the cell model undergoes aging. Experimentations demonstrated that the SVSF produces more accurate SOC estimates over the EKF for uncertain scenarios. The other advantage of the SVSF method for SOC estimation is introducing a new performance indicator referred to as the chattering indicator. This indicator measures uncertainties in the SOC estimation. It is used as an indicator for SOH estimation without the need to model the aged cell. Aging tests confirm the accuracy of the chattering indicator for SOH estimation of the Lithium polymer cell under uncertain and unmodeled aging conditions. It is important to note that the presented SOH estimation method would be applicable for different battery chemistries.

Acknowledgment

The authors gratefully acknowledge the support from Cadex Electronics Inc. and the Centre for Mechatronics and Hybrid Technologies at McMaster University. This research was financially supported by Natural Science and Engineering Research Council of Canada (NSERC-NSERC Engage 2016).

References

Afshari, H., Ahmed, R., Farag, M., & Habibi, S. (2016). Dynamic analysis of a Li-Iron phosphate cell using the electro-chemical modelling approach. In *2016 IEEE ITEC conference*, Dearborn, MI, US.

Afshari, H., Al-Ani, D., & Habibi, S. (2014). Fault prognosis of roller bearings using the adaptive auto-step reinforcement learning technique. In *ASME dynamic systems and control conference, DSCC2014-6108*, San Antonio, Texas, US.

Afshari, H., Al-Ani, D., & Habibi, S. (2015). State estimation of a faulty actuator using the second-order smooth variable structure filter (the 2nd-order SVSF). In *28th IEEE canadian conference on electrical and computer engineering* Halifax, Canada.

Afshari, H. H., Attari, M., Ahmed, R., Farag, M., & Habibi, S. R. (2016). Modeling, parameterization, and state of charge estimation of li-ion cells using a circuit model. In *IEEE transportation electrification conference and expo (ITEC)*, Dearborn, MI, USA.

Afshari, H., Gadsden, S., & Habibi, S. (2014). Robust fault diagnosis of an electro-hydrostatic actuator using the novel optimal second-order SVSF and IMM strategies. *International Journal of Fluid Power*, *15*(3), 81–196.

Afshari, H., Gadsden, A., & Habibi, S. (2017). Gaussian filters for parameter and state estimation: a general review of theory and recent trends. *Signal Processing*, *135*, 218–238.

Afshari, H., Gadsden, A., & Habibi, S. (2018). A nonlinear second-order filtering strategy for state estimation of uncertain systems. *Signal Processing* (in press).

Ahmed, R., El-Sayed, M., Arasaratnam, I., & Habibi, S. (2014). Reduced-order electrochemical model parameter identification and SOC estimation for healthy and aged Li-Ion batteries, Part 1: Parametrization model development for healthy batteries. *IEEE Transactions on Emerging and Selected Topics in Power Electronics*, *2*(3), 678–690.

Ahmed, R., El-Sayed, M., Arasaratnam, I., Tjong, J., & Habibi, S. (2014). Reduced-order electrochemical model parameter identification and soc estimation for healthy and aged li-ion batteries, part 2: aged battery model and state of charge estimation. *IEEE Transactions on Emerging and Selected Topics in Power Electronics*, *2*(3), 678–690.

Al-Ani, D. (2012). *Energy optimization strategy for system-operational problems*. (Ph.D. thesis), Hamilton, ON, Canada: Department of Mechanical Engineering, McMaster University.

Arasaratnam, I., & Haykin, S. (2009). Cubature Kalman filters. *IEEE Transactions on Automatic Control*, *54*(6), 1254–1269.

Chen, X., Shen, W., Dai, M., Cao, Z., Jin, J., & Kapoor, A. (2016). Robust adaptive sliding-mode observer using RBF neural network for lithium-ion battery state of charge estimation in electric vehicles. *IEEE Transactions on Vehicular Technology*, *65*(4), 1936–1947.

Ferrari-Trecate, G., Muselli, M., Liberati, D., & Morari, M. (2003). A clustering technique for the identification of piecewise affine systems. *Automatica*, *39*(2), 205–217.

Gadsden, S. A., & Habibi, S. (2013). A new robust filtering strategy for linear systems. *ASME Journal of Dynamic Systems, Measurement, and Control*, *135*(1), 014503.

Gandhi, M. A., & Mili, L. (2010). Robust Kalman filter based on a generalized maximum-likelihood-type estimator. *IEEE Transactions on Signal Processing*, *58*(5), 2509–2520.

Gomez, J., Nelson, R., Kalu, E. E., Weatherspoon, M. H., & Zhang, J. P. (2011). Equivalent circuit model parameters of a high-power Li-ion battery: thermal and state of charge effects. *Journal of Power Sources*, *196*, 4826–4831.

Habibi, S. (2007). Smooth variable structure filter. *Proceedings of the IEEE*, *95*(5), 1026–1059.

Hu, X., Li, S., & Peng, H. (2012). A comparative study of equivalent circuit models for Li-Ion batteries. *Journal of Power Sources*, *198*, 359–367.

Kim, J., & Cho, B. H. (2011). State-of-charge estimation and state-of-health prediction of a Li-Ion degraded battery based on an EKF combined with a per-unit system. *IEEE Transactions on Vehicular Technology*, *60*(9), 4249–4260.

Krener, A. J. (1980). Kalman-Bucy and minimax filtering. *IEEE Transactions on Automatic Control*, *25*(2), 291–292.

Lashway, C. R., & Mohammed, O. A. (2016). Adaptive battery management and parameter estimation through physics-based modeling and experimental verification. *IEEE Transactions on Transportation Electrification*, *2*(4), 454–464.

Milanese, M., & Tempo, R. (1985). Optimal algorithms theory for robust estimation and prediction. *IEEE Transactions on Automatic Control*, *30*(8), 730–738.

Plett, G. L. (2004a). Extended Kalman filtering for battery management systems of LiPB-based HEV battery packs: Part 1: Background. *Journal of Power Sources*, *134*(2), 252–261.

Plett, G. L. (2004b). Extended Kalman filtering for battery management systems of LiPB-based HEV battery packs: Part 2: Modeling and identification. *Journal of Power Sources*, *134*(2), 262–276.

Plett, G. L. (2004c). Extended Kalman filtering for battery management systems of LiPB-based HEV battery packs: Part 3: State and parameter estimation. *Journal of Power Sources*, *134*(2), 277–292.

Rahimi-Eichi, H., Baronti, F., & Chow, M. Y. (2014). Online adaptive parameter identification and state-of-charge estimation for lithium-polymer battery cells. *IEEE Transactions on Industrial Electronics*, *61*(4), 2053–2061.

Ristic, B., Arulampalam, B. S., & Gordon, N. (2004). *Beyond the Kalman filter: Particle filters for tracking applications*. Boston: Artech House.

Samadani, S., Fraser, R., & Fowler, M. (2012). A review study of methods for Lithium-ion battery health monitoring and remaining life estimation in hybrid electric vehicles, SAE Technical Paper, Vols. 2012, pp. 01–0125.

The U.S. DOE/Idaho National Laboratory (2008). Battery test manual for plug-in HEVs, Idaho Falls, Idaho, US.

Zames, G. (1981). Feedback and optimal sensitivity: model reference transformations multiplicative seminorms and approximate inverse. *IEEE Transactions on Automatic Control*, *26*(2), 301–320.

Zhao, S., Duncan, S., & Howey, D. (2017). Observability analysis and state estimation of lithium-ion batteries in the presence of sensor biases. *IEEE Transactions on Control Systems Technologies*, *25*(1), 326–333.